REPORT DOCUMENTATION PAGE

1a. REPORT SECURITY CLASSIFICATION Unclassified	1b. RESTRICTIVE MARKINGS
2a. SECURITY CLASSIFICATION AUTHORITY	3. DISTRIBUTION / AVAILABILITY OF REPORT Approved for public release Distribution unlimited
2b. DECLASSIFICATION / DOWNGRADING SCHEDULE	
4. PERFORMING ORGANIZATION REPORT NUMBER(S) RU-TR-MAE-192-F	5. MONITORING ORGANIZATION REPORT NUMBER(S)
6a. NAME OF PERFORMING ORGANIZATION Dept Mech and Aero Engr Rutgers University 6b. OFFICE SYMBOL (*If applicable*)	7a. NAME OF MONITORING ORGANIZATION Air Force Office of Scientific Research
6c. ADDRESS (*City, State, and ZIP Code*) PO Box 909 Piscataway, NJ 08855-0909	7b. ADDRESS (*City, State, and ZIP Code*) Bldg 410, Bolling AFB Washington, DC 20332
8a. NAME OF FUNDING / SPONSORING ORGANIZATION Air Force Office of Scientific Research 8b. OFFICE SYMBOL (*If applicable*) AFOSR/NA	9. PROCUREMENT INSTRUMENT IDENTIFICATION NUMBER F49620-93-1-0005
8c. ADDRESS (*City, State, and ZIP Code*) Bldg 410, Bolling AFB Washington, DC 20332 NA	10. SOURCE OF FUNDING NUMBERS PROGRAM ELEMENT NO. 2307AS; PROJECT NO. 2307; TASK NO. A5; WORK UNIT ACCESSION NO.
11. TITLE (*Include Security Classification*) Theoretical Investigation of 3-D Shock Wave Turbulent Boundary Layer Interactions (Unclassified)	
12. PERSONAL AUTHOR(S) Doyle D. Knight	
13a. TYPE OF REPORT Final	13b. TIME COVERED FROM 92/10/1 TO 96/7/31
14. DATE OF REPORT (*Year, Month, Day*) 96/9/18	15. PAGE COUNT 47
16. SUPPLEMENTARY NOTATION AFOSR-TR-96 0513	

17. COSATI CODES		
FIELD	GROUP	SUB-GROUP

18. SUBJECT TERMS (*Continue on reverse if necessary and identify by block number*)
High speed flows; shock/boundary layer interactions; computational fluid dynamics; Navier-Stokes; turbulence

19. ABSTRACT (*Continue on reverse if necessary and identify by block number*)

This report summarizes the research project "Theoretical Investigation of 3-D Shock Wave - Turbulent Boundary Layer Interactions" during the period 1 October 1992 to 31 July 1996. The principal objectives of the research are the investigation of 3-D shock wave-turbulent boundary layer interactions ("3-D turbulent interactions") for complex configurations (*e.g.*, asymmetric shock), and the investigation of the accuracy of Chien's $k-\epsilon$ turbulence model, a newly developed Reynolds Stress Equation turbulence model and a $k-\epsilon$ model with a new low Reynolds number correction for 3-D turbulent interactions, with specific focus on the ability to predict surface heat transfer and skin friction. Accomplishments during the project include the development of a Reynolds Stress Equation (RSE) model (including determination of all constants), and computation of 3-D asymmetric and symmetric shock interactions at Mach 4 using Chien's $k-\epsilon$ turbulence model, the RSE model and the $k-\epsilon$ model with the new low Reynolds number correction. The report also provides a list of publications, scientific interactions and personnel.

20. DISTRIBUTION / AVAILABILITY OF ABSTRACT ☒ UNCLASSIFIED/UNLIMITED ☐ SAME AS RPT ☐ DTIC USERS	21. ABSTRACT SECURITY CLASSIFICATION Unclassified
22a. NAME OF RESPONSIBLE INDIVIDUAL DR Leonidas Sakell	22b. TELEPHONE (*Include Area Code*) 202 767-4935 22c. OFFICE SYMBOL AFOSR/NA

DD FORM 1473, 84 MAR 83 APR edition may be used until exhausted. All other editions are obsolete.

SECURITY CLASSIFICATION OF THIS PAGE
Unclassified

19961028 008

DTIC QUALITY INSPECTED 1

Abstract

This report summarizes the research project "Theoretical Investigation of 3-D Shock Wave - Turbulent Boundary Layer Interactions" during the period 1 October 1992 to 31 July 1996. The principal objectives of the research are the investigation of 3-D shock wave-turbulent boundary layer interactions ("3-D turbulent interactions") for complex configurations (*e.g.*, asymmetric shock), and the investigation of the accuracy of Chien's $k - \epsilon$ turbulence model, a newly developed Reynolds Stress Equation turbulence model and a $k - \epsilon$ model with a new low Reynolds number correction for 3-D turbulent interactions, with specific focus on the ability to predict surface heat transfer and skin friction. Accomplishments during the project include the development of a Reynolds Stress Equation (RSE) model (including determination of all constants), and computation of 3-D asymmetric and symmetric shock interactions at Mach 4 using Chien's $k - \epsilon$ turbulence model, the RSE model and the $k - \epsilon$ model with the new low Reynolds number correction. The report also provides a list of publications, scientific interactions and personnel.

Contents

List of Figures

Chapter 1

Overview

1.1 Introduction

The design of high speed aircraft depends critically upon knowledge of turbulence. Aerodynamic forces and thermal loads are strongly affected by the turbulent flow encompassing high speed aircraft and their subsystems (*e.g.*, engines). Presently, high speed aircraft design is limited, in part, by insufficient understanding of compressible turbulent flows, and inadequate models for predicting their behavior [1, 2].

The study of **3-D shock wave-turbulent boundary layer interactions** (referred to as "3-D Turbulent Interactions") is an important area of current research in compressible turbulence. Commonly observed in high speed flight, 3-D turbulent interactions directly affect the performance of high speed aircraft. For example, shock wave-turbulent boundary layer interaction is an important consideration in all supersonic and hypersonic inlet designs [3]. Good understanding and prediction of the shock wave/turbulent boundary layer interaction will provide important information to aircraft designers. Knight recently reviewed the status of the CFD research on three-dimensional shock wave/turbulent boundary layer interaction for a family of geometries [4]. It is now generally understood that the shock wave structure and pressure field can be accurately predicted in general for simple 3-D shock wave/turbulent boundary layer interactions, e.g., sharp fin and swept compression corner. However, the heat transfer prediction remains a challenge. Typically, predicted heat transfer shows a large deviation from the experiment. Such disagreement is believed to be due to the inadequacy of the turbulence modeling. To investigate the effect of the turbulence modeling on the simulation accuracy of the 3-D Turbulent Interactions, three different turbulence models were used in this project. Among the turbulence models, the first is the popularly used Chien's $k-\epsilon$ model with low Reynolds number

correction [5]; the second is a RSE turbulence model developed in this project [6]; and the third is the $k-\epsilon$ model with the new low Reynolds number correction developed under separate sponsorship [7].

The computation of the 3-D Turbulent Interactions using the RSE model in this project [8, 9] is aimed to overcome the disadvantages of the eddy viscosity concept inherent in algebraic and $k-\epsilon$ models. Reynolds Stress Equation (RSE) turbulence models are promising since they naturally incorporate the non-local and history effects of the Reynolds stress development. However, applications of RSE models are mainly in the research field of incompressible flow. The computation is this project is the first application of RSE model to a 3-D shock wave/turbulent boundary layer interaction flow.

The two equation k–ϵ model is the still most common choice since it can in principle better predict complex flowfields than algebraic models and is significantly simpler than sophisticated higher order closures. In this research program, a $k-\epsilon$ model with a new low Reynolds number correction [7] was employed . This low Reynolds number model was developed on the basis of three principles, namely, 1) the model employs the physical dissipation rate ϵ, 2) the normal distance y is avoided, and 3) the minimum number of modifications are introduced, as described by Speziale [10]. The low Reynolds number modifications are 1) incorporation of molecular diffusion of k and ϵ, 2) modification of the turbulent eddy viscosity μ_T to provide proper asymptotic behavior near the wall, and 3) modification of the dissipation of ϵ to avoid singularities in the ϵ equation near the wall.

Since the structure of shock wave-turbulent boundary layer interactions for simple geometries is generally well understood, attention has focused in this project on more complex 3-D shock wave-turbulent boundary layer interaction, including the crossing shock (double fin) interaction (Fig. 1.1).

This configuration has been proposed as a possible hypersonic inlet [11, 12]. Most of the research work to date has focused on the symmetric crossing shock interaction [13, 14, 15, 16, 17, 18, 19, 20]. Collaborative experimental and computational research has elucidated the wave and streamline structure. Good agreement has been observed between computed and experimental surface pressure and flowfield profiles; however, computed heat transfer has been found to typically overestimate the experimental data [4, 14, 21]. Various modifications to two equation turbulence models have been tested to improve the prediction of heat transfer [20].

There are only a few studies of the asymmetric crossing shock interaction. Garrison and Settles [22] [23] obtained surface flow visualization and planar Laser Sheet images for a serious of crossing shock configurations at Mach 3.9. Zheltovodov et al [23] obtained surface pressure, heat transfer and flow visualization for several asymmetric

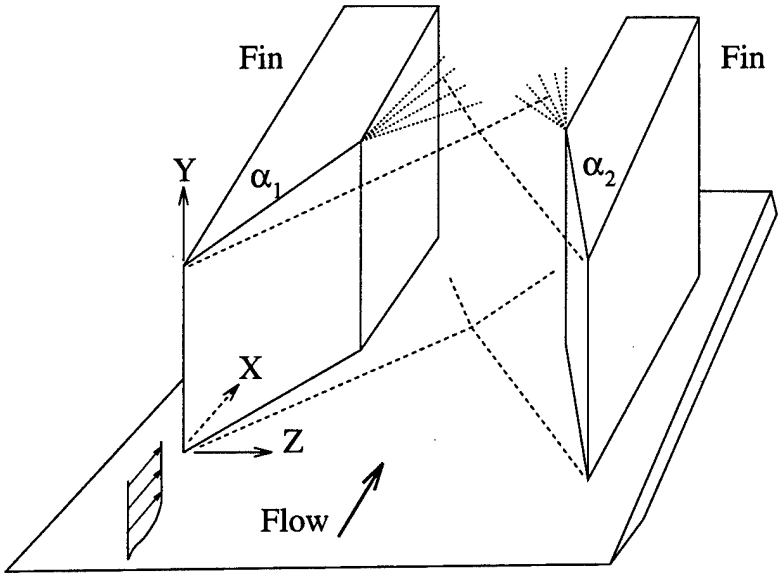

Figure 1.1: The sketch of a double fin

crossing shock interactions at Mach 3 and 4. The first computation of the 3D asymmetric crossing shock wave/turbulent boundary layer interaction was done in this research program by using Chien's $k-\epsilon$ turbulence model [24]. Good agreement was observed between computed and experimental surface pressure and flow visualization; however, surface heat transfer was over predicted by 100% within the 3-D interaction region. The newly developed RSE and $k-\epsilon$ model with low Reynolds number correction were also used to compute the asymmetric crossing shock interaction flow to examine the capability of these models to predict such complex flows.

1.2 Objectives

The objectives of the research program [25] are:

1. To study 3-D turbulent interactions in complex configurations including the asymmetric crossing shock.
2. To investigate the accuracy of the Reynolds Stress Equation turbulence model developed in this program for simulation of 3-D turbulent interactions with specific focus on prediction of surface heat transfer.
3. To investigate the accuracy of the $k-\epsilon$ turbulence model with a new low Reynolds number correction for simulation of 3-D interactions with specific

focus on prediction of surface heat transfer and skin friction.

The three year research program was initiated in October 1992. In Chapter 2, the research accomplishments for the period October 1992 through July 1996 are presented. In Chapter 3, publications and personnel are listed.

Chapter 2

Research Accomplishments: Oct '92 - July '96

2.1 Turbulence Models

2.1.1 Governing Equations

The governing equations are the Reynolds averaged Navier- Stokes equations with the additional equations for the Reynolds stresses, the turbulent dissipation rate and heat flux terms. The Reynolds-averaged Navier-Stokes equations for conservation of mass, momentum and energy are,

$$\partial_t \bar{\rho} + \partial_k \bar{\rho} \tilde{u}_k = 0 \tag{2.1}$$

$$\partial_t \bar{\rho} \tilde{u}_i + \partial_k \bar{\rho} \tilde{u}_i \tilde{u}_k = -\partial_i \bar{p} + \partial_k \left(-\overline{\rho u_i'' u_k''} + \bar{\tau}_{ik} \right) \tag{2.2}$$

$$\begin{aligned} \partial_t \bar{\rho} \tilde{e} + \partial_k \left(\bar{\rho} \tilde{e} + \bar{p} \right) \tilde{u}_k = \partial_k \left(-c_p \overline{\rho T'' u_k''} - \bar{q}_k \right) \\ + \partial_k \left(-\overline{\rho u_i'' u_k''} \tilde{u}_i + \tilde{u}_i \bar{\tau}_{ik} \right) + \partial_k \left(-\frac{1}{2} \overline{\rho u_j'' u_j'' u_k''} + \overline{u_i'' \tau_{ik}} \right) \end{aligned} \tag{2.3}$$

where $\partial_t = \partial/\partial t$, $\partial_k = \partial/\partial x_k$ and the Einstein summation convention is employed. The overbar denotes a conventional Reynolds average, while the tilde is used to denote the Favre mass average. A double superscript $''$ represents fluctuations with respect

to the Favre average, while a single superscript $'$ stands for fluctuations with respect to the Reynolds average.

In above equations, $\bar{\rho}$ is the mean density, $\tilde{u}_i$ is the mass-averaged Cartesian velocity with $(\tilde{u}_1, \tilde{u}_2, \tilde{u}_3) = (\tilde{u}, \tilde{v}, \tilde{w})$, $\bar{p}$ is the mean pressure, and $\tilde{e}$ is the mass-averaged total energy per unit mass. The following relations are employed to evaluate $\bar{p}$ and $\tilde{e}$:

$$\bar{p} = \bar{\rho} R \tilde{T} \tag{2.4}$$

$$\tilde{e} = c_v \tilde{T} + \frac{1}{2}\tilde{u}_i \tilde{u}_i + k \tag{2.5}$$

where k is the mass-averaged turbulence kinetic energy

$$\bar{\rho} k = \frac{1}{2}\overline{\rho u_i'' u_i''} \tag{2.6}$$

The mean molecular viscous stress $\bar{\tau}_{ij}$ is

$$\bar{\tau}_{ij} = -\frac{2}{3}\tilde{\mu}\,\partial_k \tilde{u}_k \delta_{ij} + \tilde{\mu}\left(\partial_i \tilde{u}_j + \partial_j \tilde{u}_i\right) \tag{2.7}$$

where $\tilde{\mu} \equiv \mu(\tilde{T})$ is determined by the Sutherland law. Similarly, the molecular heat flux is

$$\bar{q}_k = -\frac{c_p \tilde{\mu}}{Pr}\partial_k \tilde{T} \tag{2.8}$$

where Pr is the molecular Prandtl number.

In the energy equation, the triple velocity correlation $\frac{1}{2}\overline{\rho u_j'' u_j'' u_k''}$ and the velocity-molecular shear correlation $\overline{u_i'' \tau_{ik}}$ are considered small and are neglected [26].

To close the above equations, a turbulence model needs to be introduced to determine the Reynolds stress $-\overline{\rho u_i'' u_j''}$ and turbulent heat flux $-c_p\overline{\rho T'' u_i''}$. Chien's $k-\epsilon$ turbulence model, a RSE model and the $k-\epsilon$ turbulence model with the new low Reynolds number correction developed by Knight were used to compute the above Reynolds stress terms. The following section presents each turbulence model used in this program in detail. The above governing equations were solved by using Roe's upwind scheme for convective and pressure terms and central differencing for the viscous terms. Implicit approximation factorization method was used to integrate the governing equations in temporal direction [24, 27, 28].

2.1.2 A Reynolds Stress Equation Turbulence Model

A full Reynolds Stress Equation (RSE) turbulence model developed by Knight[6] is employed. The model is an extension of an incompressible flow RSE model to

its compressible counterparts with some modification regarding the compressibility effects. The model is presented below.

The equation for the Reynolds stress is,

$$\partial_t \overline{\rho u_i'' u_j''} + \partial_k \overline{\rho u_i'' u_j''} \tilde{u}_k = A_{ij} + B_{ij} + C_{ij} + D_{ij} \tag{2.9}$$

where the A_{ij}, B_{ij}, C_{ij} and D_{ij} are the Reynolds stress production term, diffusion term, pressure-rate of strain correlation and dissipation term. They are expressed as:

$$A_{ij} = -\overline{\rho u_j'' u_k''} \partial_k \tilde{u}_i - \overline{\rho u_i'' u_k''} \partial_k \tilde{u}_j \tag{2.10}$$

$$B_{ij} = \partial_k \left\{ -\overline{\rho u_i'' u_j'' u_k''} + \overline{u_j'' \tau_{ik}} + \overline{u_i'' \tau_{jk}} - \overline{p u_i''} \delta_{jk} - \overline{p u_j''} \delta_{ik} \right\} \tag{2.11}$$

$$C_{ij} = \overline{p \left(\partial_j u_i'' + \partial_i u_j'' \right)} \tag{2.12}$$

$$D_{ij} = -\overline{\tau_{ik} \partial_k u_j''} - \overline{\tau_{jk} \partial_k u_i''} \tag{2.13}$$

The production term of the Reynolds stress requires no further modeling since the Reynolds stress and mean velocity are dependent variables.

In the RSE model, the diffusion term is modeled as:

$$\begin{aligned} B_{ij} = \; & \partial_k \left\{ C_{d_1} \frac{k}{\bar{\rho}\epsilon} \left\{ \overline{\rho u_i'' u_m''} \partial_m \left(\overline{\rho u_j'' u_k''} \right) + \overline{\rho u_j'' u_m''} \partial_m \left(\overline{\rho u_i'' u_k''} \right) + \overline{\rho u_k'' u_m''} \partial_m \left(\overline{\rho u_i'' u_j''} \right) \right\} \right\} \\ + \; & \partial_k \left\{ \tilde{\nu} \left\{ \partial_k \left(\overline{\rho u_i'' u_j''} \right) + \partial_j \left(\overline{\rho u_i'' u_k''} \right) + \partial_i \left(\overline{\rho u_j'' u_k''} \right) \right\} \right\} \end{aligned} \tag{2.14}$$

where $\tilde{\nu} \equiv \tilde{\mu}/\bar{\rho}$ and C_{d_1} is a constant. This model is an extension of the incompressible flow model of Launder, Reece and Rodi [29]

The correlation of the instantaneous pressure and fluctuating rate-of-strain is modeled as:

$$C_{ij} = -C_{p_1} \frac{\epsilon}{k} \left\{ \overline{\rho u_i'' u_j''} - \frac{2}{3} \bar{\rho} k \delta_{ij} \right\} + C_{p_2} \bar{\rho} k \left\{ \partial_j \tilde{u}_i + \partial_i \tilde{u}_j \right\} \tag{2.15}$$

where C_{p_1} and C_{p_2} are constants. This is an extension of Rotta's model [30] for incompressible flow.

An isotropic dissipation model with compressibility effect is used to determine the dissipation term:

$$D_{ij} = -\frac{2}{3} \bar{\rho} \epsilon \delta_{ij} \tag{2.16}$$

According to Sarkar et al. [31] and Zeman [32]

$$\bar{\rho}\epsilon = \bar{\rho}\left(\epsilon_s + \epsilon_c\right)$$

where $\epsilon_c = C_k \epsilon_s M_t^2$ and the turbulence Mach number is $M_t = \sqrt{2k}/\tilde{a}$. Even though this compressible flow effect for dissipation is incorporated in the computer code, it is actually not used and the $C_k = 0$ because, for wall bounded flows, this effect is small and the above modification is also questionable [33].

The conventional equation [34] is employed for ϵ_s,

$$\partial_t \bar{\rho}\epsilon_s + \partial_k \bar{\rho}\epsilon_s \tilde{u}_k = -C_{\epsilon_1}\frac{\epsilon_s}{k}\overline{\rho u_i'' u_k''}\partial_k \tilde{u}_i - C_{\epsilon_2}\bar{\rho}\frac{\epsilon_s^2}{k} + \partial_k\left\{\left(C_{\epsilon_3}\bar{\rho}\frac{k^2}{\epsilon} + \tilde{\mu}\right)\partial_k \epsilon_s\right\} \quad (2.17)$$

where C_{ϵ_1}, C_{ϵ_2} and C_{ϵ_3} are constants.

The turbulent heat flux is modeled using a gradient diffusion hypothesis

$$-c_p\overline{\rho T'' u_i''} = c_p\,\bar{\rho}\,C_h\frac{k^2}{\epsilon}\partial_i \tilde{T} \quad (2.18)$$

where C_h is a constant.

Table 2.1 presents the values of the closure constants of the present RSE turbulence model [35].

Table 2.1: Turbulence Model Constants

Quantity	Value
C_{d_1}	0.086
C_{p_1}	4.325
C_{p_2}	0.179
C_{ϵ_1}	1.01
C_{ϵ_2}	1.80
C_{ϵ_3}	0.10
C_k	0.0
C_h	0.0857

There are two ways to treat the flow field in the vicinity of the walls: one is to use wall functions and the other is to use the low Reynolds number correction to resolve the viscous sublayer. The wall function method is chosen in this paper to save

computational time. The asymptotic solutions of the above governing equations in the fully turbulent region of a 2-D boundary layer are obtained in [36]. The asymptotic solutions (wall functions) are:

$$\frac{\tilde{u}}{u_\infty} - \frac{1}{2A^2}\left\{B + \sqrt{B^2+4A^2}\sin\left[A\frac{\bar{u}_*}{u_\infty \kappa}\left(\log y^+ + B'\kappa\right) - \arcsin\left(\frac{B}{\sqrt{B^2+4A^2}}\right)\right]\right\} = 0, \tag{2.19}$$

where

$$y^+ = \frac{y\bar{u}_*\bar{\rho}_w}{\tilde{\mu}_w}$$

$$A^2 = Pr_t\frac{(\gamma-1)}{2}M_\infty^2\frac{T_\infty}{\tilde{T}_w}$$

$$B = -Pr_t\frac{\bar{q}_w U_\infty}{c_p\bar{\tau}_w\tilde{T}_w}$$

$$B' = 5.0,$$

$$\kappa = 0.41,$$

$$\frac{\bar{\rho}_w}{\bar{\rho}} - 1 - B\frac{\tilde{u}}{u_\infty} + A^2\left(\frac{\tilde{u}}{u_\infty}\right)^2 = 0 \tag{2.20}$$

$$\bar{p} = \bar{R}\bar{\rho}_w\tilde{T}_w \tag{2.21}$$

$$\mathrm{k}_{iso}\left(\tilde{T}_w - \tilde{T}_{wall}\right) + (1-\mathrm{k}_{iso})\left(\bar{q}_w - \bar{q}_{wall}\right) = 0. \tag{2.22}$$

$$\epsilon - \frac{\alpha_4\bar{u}_*^3}{y}\left(\frac{\bar{\rho}_w}{\bar{\rho}}\right)^{1.5} = 0, \tag{2.23}$$

$$\overline{\rho u'' u''} - \alpha_1\bar{\tau}_w = 0 \tag{2.24}$$

$$\overline{\rho v'' v''} - \alpha_2\bar{\tau}_w = 0 \tag{2.25}$$

$$\overline{\rho w'' w''} - \alpha_3\bar{\tau}_w = 0 \tag{2.26}$$

$$\overline{\rho u'' v''} + \bar{\tau}_w = 0 \tag{2.27}$$

$$\tilde{v} = \tilde{w} = 0 \tag{2.28}$$

where $Pr_t = 0.9$, u_∞ and T_∞ are reference velocity and temperature. $\mathrm{k}_{iso} = 1$ indicates a specified wall temperature and $\mathrm{k}_{iso} = 0$ implies a specified wall heat flux. The constants α_1, α_2 , α_3 and α_4 are defined as:

$$\alpha_1 = (C_{p_1}+2)\sqrt{\frac{2}{3\left(C_{p_1}-1-1.5C_{p_1}C_{p_2}\right)}} \tag{2.29}$$

$$\alpha_2 = \frac{C_{p_1} - 1}{C_{p_1} + 2}\alpha_1 \tag{2.30}$$

$$\alpha_3 = \alpha_2 \tag{2.31}$$

$$\alpha_4^2 = \frac{C_{\epsilon_3}\alpha^2}{\frac{C_{\epsilon_2}}{\alpha} - \frac{C_{\epsilon_1}C_{p_1}}{(\alpha_2 - C_{p_2}\alpha)\alpha^2}} \tag{2.32}$$

where $\alpha = \frac{1}{2}(\alpha_1 + \alpha_2 + \alpha_3)$.

These wall functions are extended in a straightforward manner to 3-D flow under the assumption that the turbulent shear stress is locally aligned with the direction of the mean flow velocity at the point of application of the wall functions. The correction to the wall functions due to the pressure gradient [37] is omitted. The relative contribution of the pressure gradient terms to the Reynolds shear stress at the point of application of the wall functions [37] is proportional to y and thus decreases with decreasing y. As indicated in [27], the computed flowfield was found to be insensitive to the y-value of the point of application of the wall functions, and thus it is concluded that the pressure gradient correction to the wall functions would have a small effect on the computed flowfield.

2.1.3 $k - \epsilon$ Turbulence Model with Chien's Low Reynolds Number Correction

In this research program, Chien's low Reynolds number $k-\epsilon$ turbulence model was firstly used to compute the 3-D asymmetric crossing shock/turbulent boundary layer interaction. This model is represented by the two-equation Jones-Launder ($k-\epsilon$) [38] turbulence model incorporating the low Reynolds number modifications of Chien [5] and extension to compressible flow [39]. The standard values of the turbulence model constants were employed [37] (Table 2.2).

The turbulence model equations in Cartesian notation are

$$\partial_t \rho k + \partial_k \rho k u_k = P_k + \partial_k \left[\left(\frac{\mu_t}{\sigma_k} + \mu \right) \partial_k k \right] - \rho \left(\epsilon + 2\nu k n^{-2} \right) \tag{2.33}$$

$$\partial_t \rho \epsilon + \partial_k \rho \epsilon u_k = C_1 \frac{\epsilon}{k} P_k + \partial_k \left[\left(\frac{\mu_t}{\sigma_\epsilon} + \mu \right) \partial_k \epsilon \right] - \rho \frac{\epsilon}{k} \left(C_2 f \epsilon + 2\nu k n^{-2} e^{-C_4 n^+} \right) \tag{2.34}$$

where ρ is the mean density, u_k is the mass-averaged velocity, k is the mass-averaged turbulence kinetic energy, ϵ is the mean rate of dissipation of k, μ_t is the turbulent eddy viscosity, μ and ν are the mean molecular dynamic and kinematic viscosity,

Table 2.2: Turbulence Model Constants

Constant	*Value*	*Constant*	*Value*
C_μ	0.09	C_4	0.5
C_1	1.35	σ_k	1.0
C_2	1.80	σ_ϵ	1.3
C_3	0.0115	Pr_t	0.9

respectively, $u_* \equiv \sqrt{\tau_w/\rho_w}$ is the friction velocity, $\partial_t \equiv \partial/\partial t$, $\partial_k \equiv \partial/\partial x_k$, and the Einstein summation notation is assumed.

The production of turbulence kinetic energy is

$$P_k = \mu_t \left(\partial_k u_j + \partial_j u_k\right) \partial_k u_j$$

where the turbulent eddy viscosity is

$$\mu_t = C_\mu \rho \frac{k^2}{\epsilon} \left(1 - e^{-C_3 n^+}\right)$$

The dimensionless damping function f is

$$f = 1 - 0.22 e^{-\left(k^2/6\nu\epsilon\right)^2}$$

The distance n is measured normal to the nearest surface, and the dimensionless distance $n^+ \equiv n u_*/\nu$.

2.1.4 $k-\epsilon$ Turbulence Model with Low Reynolds Number Correction of Knight

The high Reynolds number form of the two-equation $k-\epsilon$ model of Jones and Launder [38], extended formally to compressible flow and employing the compressibility correction of Sarkar *et al* [31] and Zeman [32], was utilized to close the Reynolds-averaged equations (2.1) to (2.3). The low Reynolds number correction developed by Knight [7] employs the physical dissipation rate $\tilde{\epsilon}$, avoids the normal distance y and utilizes the minimum number of modifications to the $k-\epsilon$ model, as described by Speziale [10]. The modifications to the standard $k-\epsilon$ model include incorporation of molecular diffusion into both turbulent transport equations, multiplication of the turbulent eddy viscosity by a factor f_μ to provide the correct asymptotic behavior of

the turbulent stresses close to a solid boundary, and the inclusion of the dimensionless function f_2 for the dissipation term in the solenoidal dissipation transport equation. The governing equations are

$$\partial_t \bar{\rho}\tilde{k} + \partial_i \bar{\rho}\tilde{k}\tilde{u}_i = -\overline{\rho u_i'' u_j''}\partial_j \tilde{u}_i - \bar{\rho}\tilde{\epsilon} + \partial_i \left(\frac{\mu_T}{\bar{\rho}\sigma_k}\partial_i \bar{\rho}\tilde{k} + \tilde{\mu}\partial_i \tilde{k} \right) \tag{2.35}$$

$$\partial_t \bar{\rho}\tilde{\epsilon}_v + \partial_i \bar{\rho}\tilde{u}_i\tilde{\epsilon}_v = -C_{\epsilon 1}\frac{\tilde{\epsilon}_v}{\tilde{k}}\overline{\rho u_i'' u_j''}\partial_j \tilde{u}_i - C_{\epsilon 2} f_2 \bar{\rho}\frac{\tilde{\epsilon}_v^2}{\tilde{k}} + \partial_i \left[\left(\frac{\mu_T}{\sigma_\epsilon} + \tilde{\mu} \right) \partial_i \tilde{\epsilon}_v \right] \tag{2.36}$$

Here the dimensionless function f_2 is taken to be $f_2 = 1 - e^{-C_{\epsilon 3}\sqrt{R_t}}$ where R_t is the turbulence Reynolds number $R_t = \bar{\rho}\tilde{k}^2/\tilde{\mu}\tilde{\epsilon}$. The dimensionless function f_μ is available in tabular form as a function of R_t, where $f_\mu = \mathcal{O}(y^{-1})$ as $y \to 0$ and $f_\mu \to 1$ as $y \to \infty$.

The standard values for the high Re number turbulence model constants were utilized [37]. The constant C_k was taken to be zero, since the turbulence Mach number in the present computations is small and consequently the dilatational dissipation can be neglected [40]. The determination of constant C_{ϵ_3} is described in detail in [7]. All turbulence constants are listed in Table 2.3.

Table 2.3: Standard $k-\epsilon$ Model Constants

Constant	*Value*
C_μ	0.09
C_{ϵ_1}	1.44
C_{ϵ_2}	1.92
Pr_t	0.9
σ_k	1.0
σ_ϵ	1.3
C_{ϵ_3}	0.17

The boundary conditions for the turbulence variables at a solid boundary are

$$\begin{aligned} \tilde{k} &= 0 \\ \tilde{\epsilon}_v &= \frac{2\tilde{\mu}_w}{\bar{\rho}_w}\left(\frac{\partial\sqrt{k}}{\partial y}\right)^2 \end{aligned} \tag{2.37}$$

where y is the normal distance to the boundary and the subscript w implies evaluation at the wall. These boundary conditions are exact.

2.2 Crossing-Shock Interaction

The following sections only give a part of the representative results. Detailed results can be seen in the cited references.

2.2.1 Computation of $7^\circ \times 11^\circ$ Double Fin Flow Field Using the RSE Turbulence Model

The asymmetric double fin channel was calculated using the RSE turbulence model [8, 27]. The two fins have angles of 7^0 and 11^0, respectively. The Mach number of the upstream flow is 3.95. The thin boundary layers on the fin surfaces were not resolved, and slip boundary conditions were applied at the fin surfaces. Previous studies of the single fin interactions [41] have demonstrated that the bottom wall shock wave - turbulent boundary layer interaction is essentially unaffected by the boundary layer on the fin. Of course, sufficiently far downstream of the intersection of the crossing shocks, the shocks will interact with the turbulent boundary layers on the sidewall fin surfaces. However, in the present study, nearly all of the experimental data is obtained upstream of the sidewall shock wave-turbulent boundary layer interactions, and consequently the omission of the fin boundary layers does not affect comparison with the experiment in this regard. Also, Bardina and Coakley [21] observed that the treatment of the fin boundary layers as laminar/turbulent affected the flowfield in the immediate vicinity of the fin/plate junction for a Mach 8.3 crossing shock interaction. However, in the present study, experimental data is available only in the central portion of the flow, and thus our comparison with experiment is expected to be unaffected by the use of slip boundary conditions on the fins.

A boundary layer equation code with the same RSE turbulence model [6] was used to generate the upstream variable profiles. Table 2.4 presents the flow parameters for the computations.

As the baseline case, the first computation for this asymmetric double fin flow used a mesh size equal to $101 \times 69 \times 49$ in the x-, y- and z-directions. The y^+ of the first grid point adjacent to the wall was equal to 28.96 at the inflow boundary. A series of computations were carried out to test the dependence of the present RSE model on the grid refinement, upstream profiles and wall temperature. Those results were compared with this baseline case and indicated that the mesh resolution of the base line case was sufficient [8, 27]. Table 2.5 provides the mesh size information for the baseline case and grid refinement cases.

The experimental data was obtained by Zheltovodov and his colleagues at the Insti-

Table 2.4: Flow Conditions

Parameter	Experiment	Computation
M_∞	3.95	3.95
$Re_{\delta\infty}$	3.033×10^5	3.033×10^5
$\delta^*_\infty(m)$	1.12×10^{-3}	1.12×10^{-3}
$\theta_\infty(m)$	1.3×10^{-4}	1.246×10^{-4}
$C_{h\infty}$	7.9×10^{-4}	5.91×10^{-4}
$p_{t\infty}$ (MPa)	1.492	1.492
$T_{t\infty}{}^0K$	260.4	260.4

tute of Theoretical and Applied Mechanics, Russian Academy of Sciences, Novosibirsk [23]. Fig. 2.1 shows the experimental measurement locations on the bottom surface of the channel. The location 1 is the throat middle line which is along the streamwise direction. Location 2, 3, and 4 are in spanwise direction with the streamwise position equal to 46 mm, 79 mm and 112 mm. Fig. 2.2 is the pressure distributions compared with the experiment [40] and the results using Chien's $k-\epsilon$ model [40] along the throat middle line. In Fig. 2.2, the computed pressures using both the RSE and $k-\epsilon$ model along the throat middle line agree well with the experiment except at the very end where there is a strong shock wave reflection from the sidewalls. Since the side wall is treated as inviscid, the computed reflected sidewall shock is displaced downstream of the experimental shock. This is the cause of the deviation between the computed and experimental pressure for $x > 140$ mm.

Fig. 2.3 is the computed heat transfer coefficient compared with the experiment and the computational results using Chien's $k-\epsilon$ model. The heat transfer coefficient C_h is defined as

$$C_h \equiv \frac{q_w(x,z)}{\rho_\infty U_\infty c_p \left(T_w(x,z) - T_{aw}(x,z)\right)}$$

where $q_w(x,z) \equiv -\kappa_w \partial T/\partial y$ is the wall heat flux. In the experiment, the C_h has a measurement accuracy uncertainty of $\pm 10\%$ to 15%. Two computations are needed to determine C_h, i.e., an isothermal case and an adiabatic case. For the isothermal case, the wall temperature is set to 265^0K and the local heat transfer $q_w(x,z)$ is computed. For the adiabatic case, the zero wall temperature gradient $\partial T/\partial y = 0$ is used as the boundary condition and the local adiabatic wall temperature $T_{aw}(x,z)$ is computed.

The C_h measurement locations are the same as those for the pressure. Along the throat middle line shown in Fig. 2.3, the computational results using $k-\epsilon$ model

Table 2.5: Grid Sizes for Mesh Refinement Tests

Parameter	Baseline	in x	in y	in z
N_x	101	201	101	101
N_y	69	69	137	69
N_z	49	49	49	97
y_1^+	29	29	20.9	29
Δy_1^+	6.21	6.21	2.64	6.21
y_1/δ_∞	.00326	.00326	.00237	.00326
y_{max}/δ_∞	15.51	15.51	15.51	15.51
$\Delta y_{min}/\delta_\infty$	0.007	0.007	0.003	0.007
$\Delta y_{max}/\delta_\infty$	1.16	1.16	0.621	1.16
$\Delta x/\delta_\infty$	0.5	0.25	0.5	0.5
$\Delta z_{min}/\delta_\infty$	0.2	0.2	0.2	0.1
$\Delta z_{max}/\delta_\infty$	0.4762	0.4762	0.4762	0.2881

and RSE model agree quite well with the experiment before the intersection of the shock waves. Both of the computational results are substantially higher than the experiment after the intersection of the shock wave interacting with the turbulent boundary layer. The maximum deviation of the RSE model from the experiment is 80% and the $k-\epsilon$ model is 100%. The RSE model therefore has a 20% accuracy improvement.

Fig. 2.4 shows the mean streamline structure with the computed turbulent kinetic energy contours developing from the upstream turbulent boundary layer. The turbulent kinetic energy was normalized by the free stream mean flow kinetic energy u_∞^2 and the x coordinates were normalized by the upstream boundary layer thickness. The two bulges on the first turbulent kinetic energy contours represent the initial formation of the individual vortices generated by the oblique shock wave/turbulent boundary layer interaction. These vortices converge to form a counter-rotating vortex pair. The shock wave/turbulent boundary layer interaction enhances the computed turbulence intensity by increasing the maximum value of k about 3 times from the channel entrance to exit. The turbulent region is also enlarged from the boundary layer at the entrance to about 3.5 times higher at the exit. These results are conjectures and are not verified by the experiment.

The CPU time per time step for this baseline case with the mesh size $101 \times 69 \times 49$ is 113.8s on the Cray C-90. Approximately 2000 time steps are needed to get the converged solution. The total CPU time for a converged solution is therefore

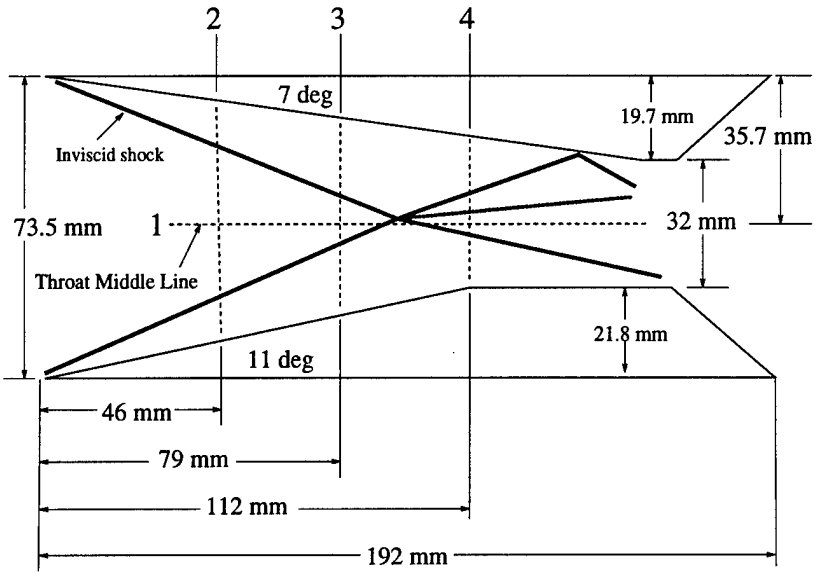

Figure 2.1: 7° × 11° double fin measurement locations: 1, 2, 3 and 4

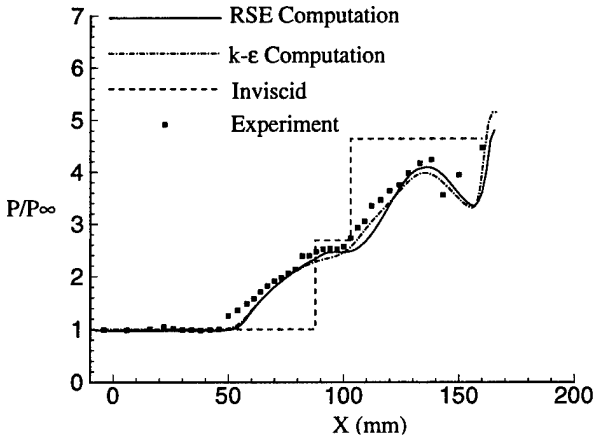

Figure 2.2: Pressure distribution along the throat middle line

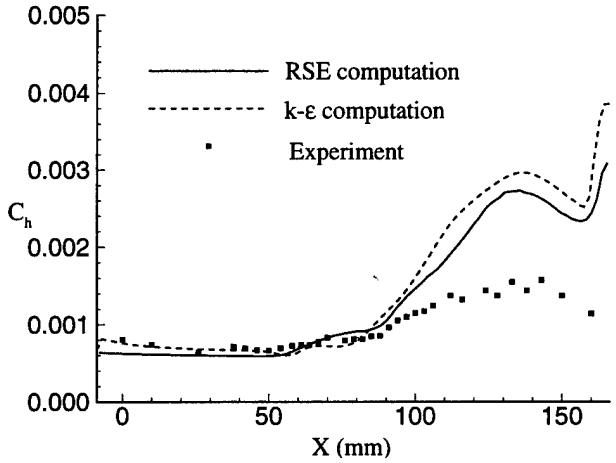

Figure 2.3: Heat transfer coefficient distribution along the throat middle line

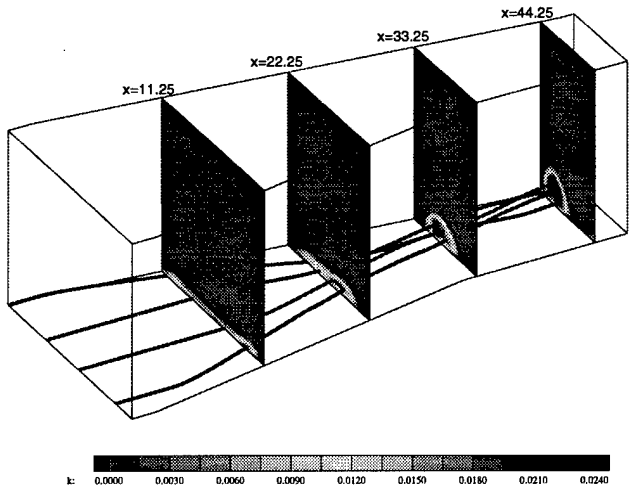

Figure 2.4: Turbulent kinetic energy contours with streamlines at different locations

approximately 63 hours. The computer code performance is 160 MFlops.

In conclusion, the computation of the flow field of a $7^0 \times 11^0$ double fin using a full RSE model obtained good agreement with the experiment for the pressure field. The computed heat transfer coefficient achieved 20% improvement compared with the results from the $k-\epsilon$ model with Chien's low Reynolds number correction. However, the maximum heat transfer coefficient still has a 80% deviation from the experiment. The computation has resolved the counter-rotating vortex pair generated by the cross shock wave/turbulent boundary layer interaction, and predicts an enhanced turbulence intensity between the vortices. The computer code with the RSE turbulence model is quite robust.

2.2.2 Computation of $7^\circ \times 11^\circ$ Double Fin Flow Field Using Chien's $k-\epsilon$ Turbulence Model

The same case was computed using the popular Chien $k-\epsilon$ Turbulence Model [40]. The following table gives the details of the computation mesh resolution.

Table 2.6: Details of Computations

Ref	α_1	α_2	T_w	N_x	N_y	N_z	$\Delta x/\delta_\infty$	$\Delta y_{min}/\delta_\infty$	$\Delta y_{max}/\delta_\infty$	$\Delta z_{min}/\delta_\infty$	$\Delta z_{max}/\delta_\infty$	$\Delta y_2^+\|_{rms}$
Case 1a	7°	11°	I	101	68	49	0.50	7.64×10^{-5}	0.51	0.20	0.48	0.16
Case 1b	7°	11°	A	101	68	49	0.50	7.64×10^{-5}	0.51	0.20	0.48	0.19

LEGEND

N_x	number of points in x	$\Delta y_2^+\|_{rms}$	rms grid spacing at wall in wall units
N_y	number of points in y	I	Isothermal wall
N_z	number of points in z	A	Adiabatic wall

The computed surface skin friction lines and experimental surface flow visualization are displayed in Figs. 2.5 and 2.6, respectively. In comparing these results here , there are two important points which must be noted. First, the computed surface skin friction lines are typically sensitive to the turbulence model employed. Second, the experimental surface flow visualization is a qualitative technique which has not been calibrated to the actual mean surface shear stress direction. Nonetheless, the comparison of these quantities is helpful in understanding the flowfield streamline structure.

The incident separation lines (lines of coalescence [42]) emanating from the fin leading edges (**1** and **2**) are clearly evident in the computation and experiment. These

separation lines are associated with the incident single fin interactions. The computed and experimental separation line angles[1] are in close agreement (Table 2.7).

The incident separation lines coalesce near the center of the region to form a narrow band of skin friction lines (**3**) offset to the left side of the channel. This line represents the surface image of the boundary between the left and right vortices generated by the incident single fin interactions. A second line of coalescence forms alongside on the right and farther downstream (**4**) associated with the appearance of a narrow layer of reversed flow underneath the left side of the right vortex as indicated in [40]. A line of divergence is also apparent near the right fin (**5**) associated with the incident single fin interaction. A similar line of divergence (unmarked) is near the left fin.

Table 2.7: Separation Line Angles

Configuration	*Reference*	β_l	β_r
$7° \times 11°$	Experiment	22°	28°
	Computation	23°	31°

LEGEND

β_l separation angle for left fin

β_r separation angle for right fin

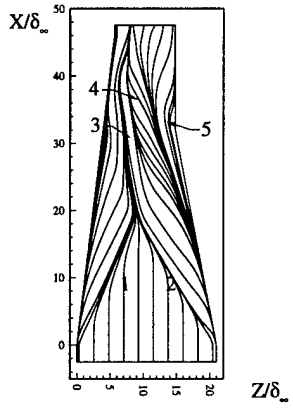

Figure 2.5: Computed skin friction lines ($7° \times 11°$)**1** Left incident separation line **2** Right incident separation line **3** Left downstream coalescence line **4** Right downstream coalescence line **5** Line of divergence (similar line near left fin)

[1]The uncertainty in determining the angle of the separation line (beyond the inception region) from the skin friction plot and surface flow visualization is $\pm 1°$.

Figure 2.6: Experimental surface flow (7° × 11°)

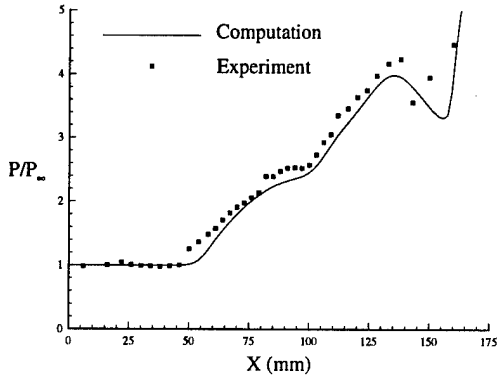

Figure 2.7: Wall pressure on TML for 7° × 11°

The surface pressure on the Throat Middle Line (TML) is shown in Fig. 2.7. Overall, good agreement is observed for $x < 135$ mm, although the computation underestimates the extent of the upstream influence, as observed in previous studies (*e.g.*, [15]). The computed pressure does not accurately predict the pressure rise (beginning at $x = 145$ mm) associated with the shock reflection from the 7° fin, since the computation omits the boundary layers on the fin surfaces.

The computed and experimental surface heat transfer coefficient C_h is presented in Fig. 2.16. Downstream of the intersection of the fin-generated $\lambda-$shock structures (*i.e.*, for $x > 90$ mm on the TML) the computations overpredict the heat transfer by approximately a factor of *two*. This discrepancy is believed attributable to the limitations of the turbulence model, and is consistent with previous results for the symmetric crossing shock at Mach 8.3 using a similar $k-\epsilon$ model [43, 44].

In conclusion, the computed surface pressure displays good agreement with experiment. The computed surface skin friction lines and experimental surface flow visualization display close agreement in the location of the initial separation lines, and are in qualitative agreement within the crossing shock interaction region. The computed heat transfer is in error by approximately a factor of *two* within the region downstream of the intersection of the $\lambda-$shocks generated by the fins.

2.2.3 Computation of Double Fins Using $k - \epsilon$ Turbulence Model with Knight's Low Reynolds Correction

The 7° × 7° and 7° × 11° fins with incoming Mach 4 were computed using the $k - \epsilon$ turbulence model with Knight's Low Reynolds Number Correction. The 7° × 11° case is the same as the one in the last two sections. The 7° × 7° fin has the same incoming flow conditions as the 7° × 11° fin. Table 2.8 gives the details of the computation mesh resolution.

The inflow profiles were generated with the boundary layer code [7], which utilizes the same turbulence model. The appropriate inflow profile is considered to be the one created by the boundary layer code which matches the experimental value of displacement thickness.

For the 7° × 7° and 7° × 11° configurations, the thin boundary layers on side walls can be neglected since the reflected shock waves intersect the sidewalls near the exit or not at all [40, 45].

Table 2.8: Details of Computations

Ref	α_1	α_2	BC	T_w	N_x	N_y	N_z
Case 1a	7°	7°	S	I	101	79	49
Case 1b	7°	7°	S	A	101	79	49
Case 2a	7°	11°	S	I	101	81	49
Case 2b	7°	11°	S	A	101	81	49
Case 2c	7°	11°	S	I	202	81	49
Case 2d	7°	11°	S	I	101	162	49
Case 2e	7°	11°	S	I	101	81	98
Case 2f	7°	11°	S	I	101	81	49

Ref	$\Delta x/\delta_\infty$	$\Delta y_{min}/\delta_\infty$	$\Delta y_{max}/\delta_\infty$	$\Delta z_{min}/\delta_\infty$	$\Delta z_{max}/\delta_\infty$	$\Delta y_2^+\|_{rms}$	$\Delta y_2^+\|_{aver}$
Case 1a	0.5	2.2×10^{-4}	0.5	0.2	0.5	0.55	0.52
Case 1b	0.5	2.2×10^{-4}	0.5	0.2	0.5	0.63	0.59
Case 2a	0.5	2.2×10^{-4}	0.5	0.2	0.5	0.70	0.62
Case 2b	0.5	2.2×10^{-4}	0.5	0.2	0.5	0.80	0.72
Case 2c	0.25	2.2×10^{-4}	0.5	0.2	0.5	0.72	0.65
Case 2d	0.5	1.1×10^{-4}	0.25	0.2	0.5	0.35	0.31
Case 2e	0.5	2.2×10^{-4}	0.5	0.1	0.25	0.70	0.63
Case 2f	0.5	2.2×10^{-4}	0.5	0.2	0.5	0.68	0.60

LEGEND

N_x	number of points in x	I	Isothermal wall
N_y	number of points in y	A	Adiabatic wall
N_z	number of points in z	N	"No-slip" sidewalls
$\Delta y_2^+\|_{rms}$	rms grid spacing at wall in wall units	S	"Slip" sidewalls
$\Delta y_2^+\|_{aver}$	average grid spacing at wall in wall units		

$7^\circ \times 7^\circ$

The computed surface skin friction lines and experimental surface flow visualization for the $7^\circ \times 7^\circ$ configuration are presented in Figs. 2.8 and 2.9, respectively. The separation lines **1** and **2** originating from the fin leading edges are apparent in the computation and experiment. The computed and experimental separation line angles agree within 7%. The computed skin friction lines do not intersect, but, after changing direction, slowly converge towards each other. Two weak divergence lines **3** and **4** can be found near the fin surfaces. The computational flow pattern is completely symmetric; however, the experimental results display a slight asymmetric behavior downstream in the vicinity of the centerline.

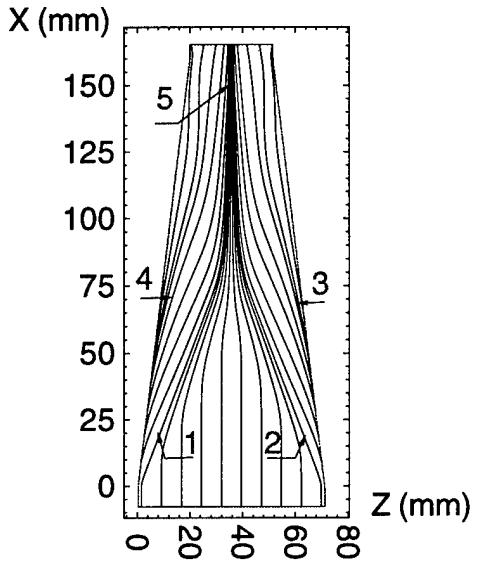

Figure 2.8: Computed skin friction lines for $7^\circ \times 7^\circ$:
1 Left incident separation line
2 Right incident separation line
3, **4** Lines of divergence
5 Downstream coalescence line

The computed and experimental surface pressure, normalized by the freestream static pressure p_∞, are displayed in Fig. 2.10 along the Throat Middle Line (TML). The uncertainty in the surface pressure measurements is $\pm 0.5\%$. The computed surface pressure displays excellent agreement with experiment.

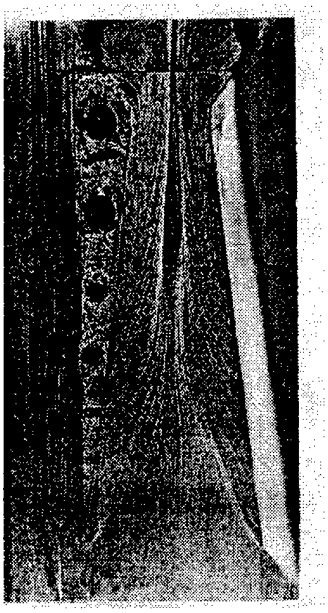

Figure 2.9: Experimental surface flow for 7° × 7°

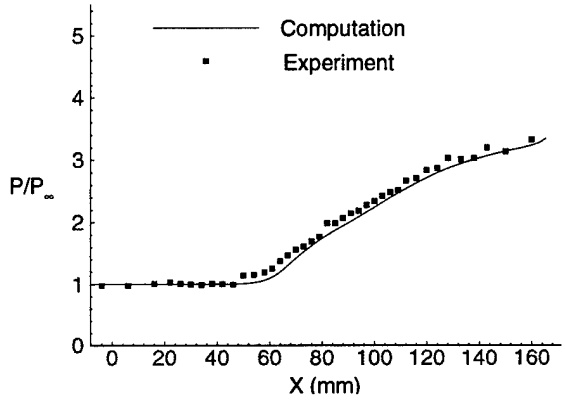

Figure 2.10: Wall pressure on TML for 7° × 7°

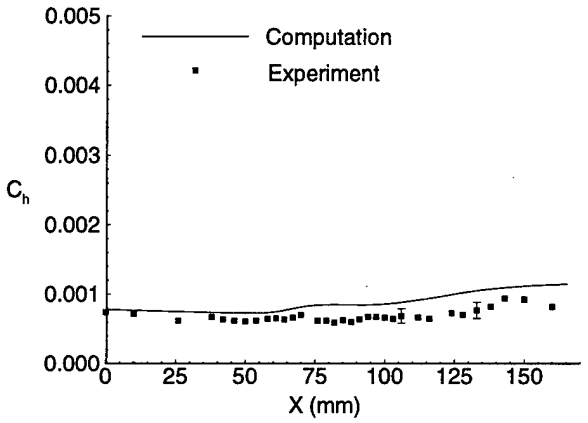

Figure 2.11: C_h on TML for 7° × 7°

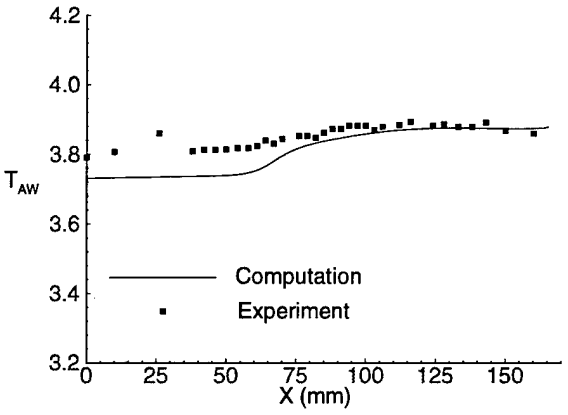

Figure 2.12: T_{aw} on TML for 7° × 7°

The computed and experimental surface heat transfer coefficient C_h is presented in Fig. 2.11. The experimental uncertainty for C_h is $\pm 10\%$ to $\pm 15\%$. Close agreement with the experiment is observed. On the TML, the heat transfer coefficient is predicted typically within 25% in the 3-D interaction region.

The adiabatic wall temperature T_{aw} is presented in Fig. 2.12 along the TML. The experimental uncertainty in T_{aw} is less than 0.2%. Close agreement is observed. The maximum difference between the predicted and measured T_{aw} is less than 2%.

$7^\circ \times 11^\circ$

For $7^\circ \times 11^\circ$ fin, the results using the $k-\epsilon$ turbulence model with Knight's low Reynolds number correction were compared with those using RSE model and the $k-\epsilon$ turbulence model with Chien's low Reynolds number correction.

Figs. 2.13 and 2.14 present the computed surface skin friction lines and experimental surface flow visualization respectively. It has been previously noted [40, 43] that the computed surface skin friction lines are sensitive to the turbulence model employed. Comparison of current results with [40], Fig. 6, shows general agreement as well as a number of substantially different details. Both incident separation lines (lines of coalescence [42]) emanating from the fin leading edges (**1** and **2**) are clearly observed in Fig. 2.13 in agreement with experimental results and previous simulations of Knight *et al* [40]. These separation lines are associated with the incident single fin interactions. The computed and experimental separation line angles, measured relative to the x-axis, agree within 9%. However, contrary to the computation with the k–ϵ Chien model [40], the incident separation lines do not coalesce near the center of the region, but rather continue further downstream almost in parallel until they converge at $x \approx 110$ mm to form a narrow band of skin friction lines (**3**), which is offset to the left side of the channel. This is denoted in [40] as the left downstream coalescence line, and represents the surface image of the boundary between the left and right vortices generated by the incident single fin interactions. The crossflow velocity vectors near the surface change direction at **3**. Lines of divergence are also apparent near the right fin (**4**) and left fin (**5**) associated with the incident single fin interaction. In a major difference with the $k-\epsilon$ Chien model results, a second line of coalescence (the right downstream coalescence line) is not present in this computation. Consequently, the model does not predict a secondary separation underneath the left side of the right vortex (see [40]). The difference is due to deviation in the predictions of the pressure distribution in the spanwise direction obtained with each turbulence model.

The computed and experimental surface pressure along the Throat Middle Line is displayed in Fig. 2.15. The computed and experimental surface pressure on TML are

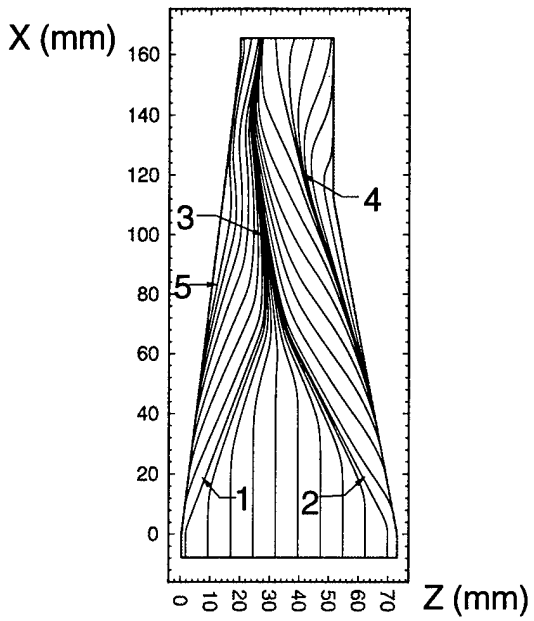

Figure 2.13: Computed skin friction lines for $7° \times 11°$:
1 Left incident separation line
2 Right incident separation line
3 Left downstream coalescence line
4,5 Lines of divergence

Figure 2.14: Experimental surface flow for $7° \times 11°$

in good agreement for $x < 135$ mm, although the computation underestimates the extent of the upstream influence, as observed in previous studies (*e.g.*, [15] [40]). The computed pressure does not accurately predict the pressure rise (beginning at $x = 145$ mm) associated with the shock reflection from the 7° fin, since all of the computations omit the boundary layers on the fin surfaces.

The computed and experimental surface heat transfer coefficient along the TML C_h is presented in Fig. 2.16. All three turbulence models overpredict the heat transfer by approximately a factor of two downstream of the intersection of the shocks (which occurs at $x = 93.7$ mm), with a modest improvement in the computations performed with RSE and present models.

The overprediction in C_h is actually an overprediction in q_w, since a series of studies [45, 46] have demonstrated that the computed q_w is proportional to the computed $T_w - T_{aw}$. A possible explanation is that the turbulence models overestimate the effects of the shock-boundary layer interaction on the turbulence production, thereby generating excessive turbulence kinetic energy and overestimating the turbulent thermal conductivity. Further experiments (in particular, measurements of the turbulence statistics within the flowfield) are needed to assist in the identification of the specific weaknesses in these models and develop improved models.

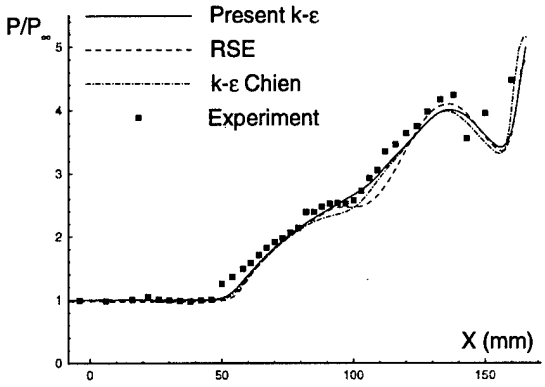

Figure 2.15: Wall pressure on TML for 7° × 11°

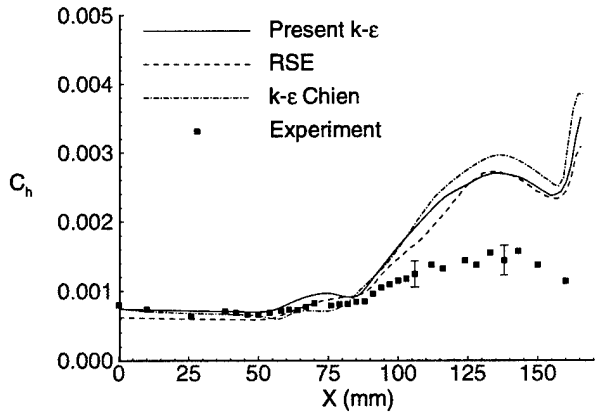

Figure 2.16: C_h on TML for 7° × 11°

The computed and experimental T_{aw} distributions in streamwise direction are displayed in Figs. 2.17. The results of the present computation exhibit excellent agreement with the experiment, and represent an improvement over the predictions by the $k-\epsilon$ Chien and RSE models [24, 27].

The computed and experimental T_{aw} contours are shown in Figs. 2.18 and 2.19, respectively. The computations used the $k-\epsilon$ model with the low Reynolds number model of Knight. The results are in qualitative agreement. The computations predict a modest increase in T_{aw} downsteam of the intersection of the incident shocks and in the vicinity of the convergence of the incident separation lines. The decrease in T_{aw} within the expansion fan originating at $x = 112$ mm is also predicted qualitatively.

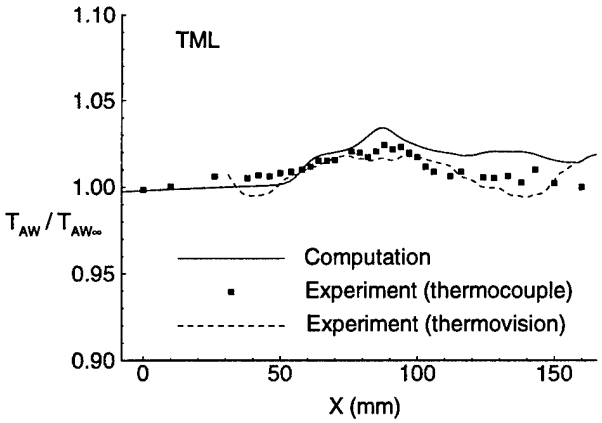

Figure 2.17: T_{aw} on TML for 7° × 11°

In conclusion, the computed surface pressure displays very good agreement with experiment for the 7° × 7° and 7° × 11° configurations. For the 7° × 11° case, similar very good agreement is obtained by the $k-\epsilon$ Chien and full RSE models. The computed surface skin friction lines are in close agreement with experiment for the initial separation lines, and are in qualitative agreement within the crossing shock interaction region. However, for the 7° × 11° case, the present model does not predict the secondary separation line. This feature is predicted by the $k-\epsilon$ Chien model. The adiabatic wall temperature is accurately predicted for all configurations. For the 7° × 11° case, the model displays a definite improvement over the $k-\epsilon$ Chien and full RSE models. The computed and experimental T_{aw} contours display qualitative agreement, including the modest increase in T_{aw} downstream of the intersection of the incident shocks and in the vicinity of the convergence of the incident separation lines, and the decrease in T_{aw} in the expansion fan.

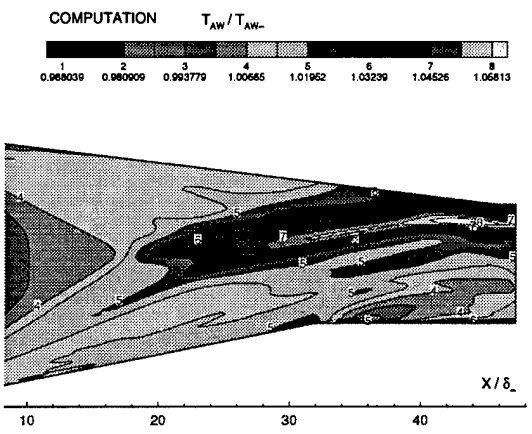

Figure 2.18: Computed T_{aw} for 7° × 11°

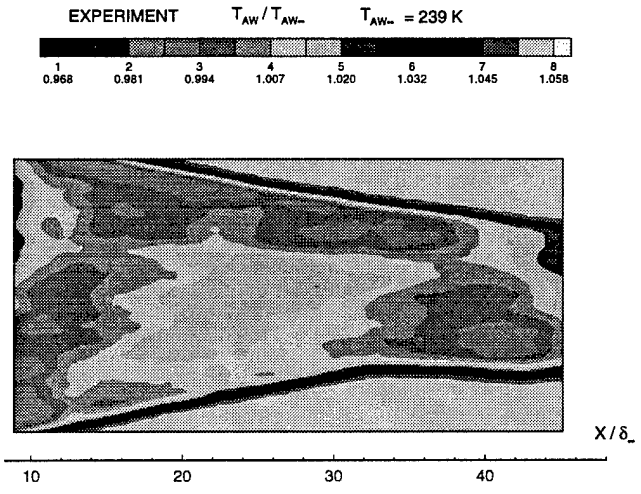

Figure 2.19: Experimental T_{aw} for 7° × 11°

2.3 Summary

The $k-\epsilon$ and Reynolds Stress Equation turbulence models demonstrated the capability for accurately predicting certain features of the flowfield for the crossing shock interaction, namely, the surface pressure and the surface flow visualization. The $k-\epsilon$ model of Knight provided an improved prediction of the surface adiabatic wall temperature. However, all three models failed to accurately predict surface heat transfer for the stronger ($7^\circ \times 11^\circ$) interaction.

Future research should focus on the investigation of more accurate turbulence models, specifically Large Eddy Simulation, for the prediction of heat transfer in shock wave turbulent boundary layer interactions.

Chapter 3

Publications and Personnel Oct '92 - Sept '96

3.1 Archival Papers

Narayanswami, N., Knight, D., and Horstman, C., "Investigation of a Hypersonic Crossing Shock Wave/Turbulent Boundary Layer Interaction" *Shock Waves*, Vol. 3, No. 1, March 1993, pp. 35-48.

Narayanswami, N., Horstman, C., and Knight, D., "Computation of Crossing Shock / Turbulent Boundary Layer Interaction at Mach 8.3", *AIAA Journal*, Vol. 31, No. 8, August 1993, pp. 1369-1376.

Garrison, T., Settles, G., Narayanswami, N., and Knight, D., "Structure of Crossing Shock Wave / Turbulent Boundary Layer Interactions", *AIAA Journal*, Vol. 31, No. 12, December 1993, pp. 2204-2211.

Garrison, T., Settles, G., Narayanswami, N., and Knight, D., "Laser Interferometer Skin-Friction Measurements of Crossing Shock Wave / Turbulent Boundary Layer Interactions", *AIAA Journal*, Vol. 32, No. 6, June 1994, pp. 1234-1241.

Knight, D., Garrison, T., Settles, G., Zheltovodov, A., Maksimov, A., Shevchenko, A., and Vorontsov, S., "Asymmetric Crossing Shock Wave - Turbulent Boundary Layer Interaction", *AIAA Journal*, Vol. 33, No. 12, December 1995, pp. 2241-2249.

Garrison, T., Settles, G., Narayanswami, N., Knight, D., and Horstman, C., "Flow-field Surveys and Computations of a Crossing-Shock Wave/Boundary Layer Interaction", *AIAA Journal*, Vol. 34, No. 1, January 1996, pp. 50-56.

G. Zha and D. Knight "Three-Dimensional Shock / Boundary-Layer Ineraction Using Reynolds Stress Equation Turbulence Model", *AIAA Journal*, Vol. 34, No. 7, July 1996, pp. 1313-1320.

3.2 Conference Papers and Reports

Narayanswami, N., Horstman, C., and Knight, D., "Numerical Simulation of Crossing Shock / Turbulent Boundary Layer Interaction at Mach 8.3", AIAA Paper No. 93-0779, January 1993.

Knight, D., Horstman, C., Settles, G., and Zheltovodov, A., "3-D Shock Wave-Turbulent Boundary Layer Interactions Generated by a Single Fin", International Center for Aerophysical Studies, Report No. 9, Institute of Theoretical and Applied Mechanics, Russian Academy of Sciences, 1993.

Garrison, T., Settles, G., Narayanswami, N., Knight, D., and Horstman, C., "Comparison of Flowfield Surveys and Computations of a Crossing-Shock Wave/Boundary Layer Interaction", AIAA Paper No. 94-2273, June 1994.

Knight, D., Garrison, T., and Settles, G., "Investigation of Asymmetric Crossing Shock Wave - Turbulent Boundary Layer Interaction", International Conference on Methods of Aerophysical Research, Institute of Theoretical and Applied Mechanics, Russian Academy of Sciences, Novosibirsk, Russia, August 1994.

Zheltovodov, A., Maksimov, A., Shevchenko, A., Vorontsov, S., and Knight, D., "Experimental Study and Computational Comparison of Crossing Shock Wave - Turbulent Boundary Layer Interaction", International Conference on Methods of Aerophysical Research, Institute of Theoretical and Applied Mechanics, Russian Academy of Sciences, Novosibirsk, Russia, August 1994.

Knight, D., Garrison, T., Settles, G., Zheltovodov, A., Maksimov, A., Shevchenko, A., and Vorontsov, S., "Asymmetric Crossing Shock Wave - Turbulent Boundary Layer Interaction", AIAA Paper No. 95-0231, January 1995.

Gnedin, M., and Knight, D., "A Reynolds Stress Turbulence Model for Compressible Flows. Part I: Flat Plate Boundary Layers", AIAA Paper No. 95-0860, January 1995.

Zha, G. and Knight, D., "Computation of 3-D Asymmetric Crossing Shock Wave / Turbulent Boundary Layer Interaction Using a Full Reynolds Stress Equation Turbulence Model", AIAA Paper No. 96-0040, January 1996.

Gnedin, M., Knight, D., Zheltovodov, A., Maksimov, A., Shevchenko, A., and Vorontsov, S., "3-D Crossing Shock Wave-Turbulent Boundary Layer Interaction", AIAA

Paper No. 96-2001, June 1996.

Gnedin, M., Zha, G., and Knight, D., "3-D Asymmetric and Symmetric Crossing Shock Wave Turbulent Boundary Layer Interactions", International Conference on Methods of Aerophysical Research, Institute of Theoretical and Applied Mechanics, Russian Academy of Sciences, Novosibirsk, Russia, September 1996.

3.3 Videotapes

Narayanswami, N., Knight, D., and Horstman, C., "Hypersonic Crossing Shock Interaction", NASA Ames Research Center, Oct 1993, 11 mins.

3.4 Presentations

"Numerical Simulation of 3-D Shock Wave-Turbulent Boundary Layer Interactions", École Polytechnique, Montreal, Québec, March 1993.

'Review of Status of Computation of 3-D Shock Wave-Turbulent Boundary Layer Interactions", Institute of Mechanics (Moscow University), TsAGI (Moscow Region), CNIIMASH (Moscow Region), CIAM (Moscow), August 1994.

"Development of a Compressible Reynolds Stress Equation Turbulence Model", University of Illinois at Urbana-Champaign, October 1994.

"Fundamental Studies of 3-D Shock Wave Turbulent Boundary Layer Interaction", Boeing Aircraft Company (WA), June 1995.

"Numerical Simulation of Shock Wave / Turbulent Boundary Layer Interactions Using Two-Equation and Full Reynolds Stress Equation Models of Turbulence", Brown University, March 1996.

3.5 Visitors to Rutgers

Dr. Doug Dwoyer, NASA Langley Research Center, January 1993.

Dr. C. C. Horstman, NASA Ames Research Center, November 1992, April 1993.

Dr. Len Sakell, Air Force Office of Scientific Research, April 1993, January 1995.

Dr. Alexander Zheltovodov, Russian Academy of Sciences, May 1994, June 1995, June 1996.

Dr. Valerie Zvegintsev, Russian Academy of Sciences, May 1994.

Dr. Nicolai Zakharov, CIAM, May 1994.

Prof. Vladimir Voul, Tupolev Design Bureau, May 1994.

3.6 List of Personnel

Graduate Student: Marianna Gnedin

Principal Investigator: Professor Doyle Knight

PhD Awarded: Marianna Gnedin, May 1996.

Bibliography

[1] D. Bushnell, "Hypervelocity Fluid Dynamics - Recent Challenges and Critical Issues." Invited Lecture, Forty Third Annual Meeting of the Division of Fluid Dynamics, American Physical Society, Bulletin of the American Physical Society, 1990. Vol. 35, No. 10, p. 2314.

[2] D. Bushnell, "Turbulence Modelling in Aerodynamic Shear Flow - Status and Problems." AIAA Paper 91-021, 1991.

[3] D. VanWie, M. White, and G. Corpening, "NASP Inlet Design and Testing Issues." Johns Hopkins APL Technical Digest, 1990.

[4] D. Knight, "Numerical Simulation of 3-D Shock Wave Turbulent Boundary Layer Interactions," in *AGARD/VKI Special Course on Shock-Wave Boundary-Layer Interactions in Supersonic and Hypersonic Flows*, pp. 3–1 to 3–32, Von Karman Institute for Fluid Dynamics, May 1993. AGARD R-792.

[5] K.-Y. Chien, "Predictions of Channel and Boundary Layer Flows with a Low Reynolds Number Turbulence Model," *AIAA Journal*, vol. 20, pp. 33–38, January 1982.

[6] M. Gnedin and D. Knight, "A Reynolds Stress Equation Model for Compressible Turbulent Flows. part i: Flat plate boundary layers." AIAA Paper No. 95-0860, 1995.

[7] C. Becht and D. Knight, "A Simple Low Reynolds Number Modification for the Compressible $k-\epsilon$ Model. Part I. Boundary Layer Flows." AIAA Paper 95-2218, 1995.

[8] G. Zha and D. Knight, "Computation of 3D Asymmetric Crossing Shock Wave / Turbulent Boundary Layer Interaction Using a Full Reynolds Stress Equation Turbulence Model." AIAA Paper No. 96-0040, 1996.

[9] G. Zha, D. Smith, M. Schwabacher, K. Rasheed, A. Gelsey, D. Knight, and M. Haas, "High Performance Supersonic Missile Inlet Design Using Automated Optimization." AIAA Paper 96-4142, 1996.

[10] C. Speziale, "Analytical Methods for the Development of Reynolds Stress Closures in Turbulence," Tech. Rep. ICASE Report No. 90-26, ICASE - NASA Langley Research Center, March 1990.

[11] C. Edwards, "A Forebody Design Technique for Highly Integrated Bottom - Mounted Scramjets with Application to a Hypersonic Research Airplane," Tech. Rep. NASA TN D-8369, December 1976.

[12] L. Sakell, D. Knight, and A. Zheltovodov, eds., *Proceedings of the AFOSR Workshop on Fluid Dynamics of High Speed Inlets*, Department of Mechanical and Aerospace Engineering, Rutgers University, New Brunswick, NJ, May 1994.

[13] D. Gaitonde, J. Shang, and M. Visbal, "Structure of a Double-Fin Interaction at High Speed," *AIAA Journal*, vol. 33, pp. 193–200, Feb 1995.

[14] N. Narayanswami, D. Knight, and C. C. Horstman, "Computation of Crossing Shock / Turbulent Boundary Layer Interaction at mach 8.3," *AIAA Journal*, vol. 31, pp. 1369–1376, August 1993.

[15] N. Narayanswami, D. Knight, S. Bogdonoff, and C. Horstman, "Interaction Between Crossing Oblique Shocks and a Turbulent Boundary Layer," *AIAA Journal*, vol. 30, pp. 1945–1952, August 1992.

[16] N. Narayanswami, D. Knight, and C. C. Horstman, "Investigation of a Hypersonic Crossing Shock Wave/Turbulent Boundary Layer Interaction," *Shock Waves*, vol. 3, pp. 35–48, 1993.

[17] T. Garrison, G. Settles, N. Narayanswami, and D. Knight, "Structure of Crossing-Shock Wave/Turbulent Boundary Layer Interactions," *AIAA Journal*, vol. 31, pp. 2204–2211, December 1993.

[18] T. Garrison and G. Settles, "Interaction Strength and Model Geometry Effects on the Structure of Crossing - Shock Wave / Turbulent Boundary - Layer Interactions." AIAA Paper 93-0780, January 1993.

[19] T. Garrison, G. Settles, N. Narayanswami, and D. Knight, "Comparison of Flowfield Surveys and Computations of a Crossing - Shock Wave / Boundary - Layer Interaction." AIAA Paper 94-2273, June 1994.

[20] J. E. Bardina and T. J. Coakley, "The Structure of Intersecting Shock-Waves/Turbulent Boundary Layer Interaction flow." AIAA Paper 95-2215, 1995.

[21] J. Bardina and T. Coakley, "Three - Dimensional Navier - Stokes Simulations with Two Equation Turbulence Models of Intersecting Shock Waves / Turbulent Boundary Layer at mach 8.3." AIAA Paper 94-1905, 1994.

[22] T. Garrison, *The Interaction Between Crossing - Shock Waves and a Turbulent Boundary Layer.* PhD thesis, Penn State University, 1994.

[23] A. Zheltovodov, A. Maksimov, A. Shevchenko, S. Vorontsov, and D. Knight, "Experimental Study and Computational Comparison of Crossing Shock Wave - Turbulent Boundary Layer Interaction," in *Proceedings of the International Conference on Methods of Aerophysical Research - Part 1*, pp. 221–230, August 1994. Russian Academy of Sciences, Siberian Division.

[24] D. Knight, T. Garrison, G. Settles, A. Zheltovodov, A. Maksimov, A. Shevchenko, and S. Vorontsov, "Asymmetric Crossing-Shock Wave / Turbulent Boundary Layer Interaction," *AIAA Journal*, vol. 33, pp. 2241–2249, Dec 1995.

[25] D. Knight, "Research in Compressible Turbulence: Development of a Reynolds Stress Equation Model and Study of 3-D Shock Wave Turbulent Boundary Layer Interactions." Three year proposal submitted to AFOSR, April 1992.

[26] D. Knight, "Numerical Simulation of 3-d Shock Wave Turbulent Boundary Layer Interactions," *Special Course on Shock-Wave/Boundary Layer Interactions in Supersonic and Hypersonic Flows, AGARD Report 792*, pp. 3–1 to 3–32. Editor: G. Degrez, Aug. 1993.

[27] G. Zha and D. Knight, "Three-Dimensional Shock / Boundary-Layer Interaction Using Reynolds Stress Equation Turbulence Model," *AIAA Journal*, vol. 34, pp. 1313–1320, July 1996.

[28] M. Gnedin, D. Knight, A. Zheltovodov, A. Maksimov, A. Shevchenko, and S. Vorontsov, "3-D Crossing Shock Waves-Turbulent Boundary Layer Interaction." AIAA Paper No. 96-2001, 1996.

[29] B. Launder, G. Reece, and W. Rodi, "Progress in the Development of a Reynolds Stress Turbulence Closure," *Journal of Fluid Mechanics*, vol. 68, pp. 537–566, 1975.

[30] J. Rotta, "Recent Attempts to Develop a Generally Applicable Calculation Method for Turbulent Shear Flows." AGARD CP-93, 1972.

[31] S. Sarkar, G. Erlebacher, M. Hussaini, and H. Kreiss, "The Analysis and Modelling of Dilatational Terms in Compressible Turbulence," *Journal of Fluid Mechanics*, vol. 227, pp. 473–493, 1991.

[32] O. Zeman, "Dilatation Dissipation: The Concept and Application in Modelig Compressible Mixing Layers," *Physics of Fluids A*, vol. 2, pp. 178–188, 1990.

[33] P. Huang, G. N. Coleman, and P. Bradshaw, "Compressible Turbulent Channel Flow- A Close Look Uuing DNS Data." AIAA Paper 95-0584, 1995.

[34] W. Jones and B. Launder, "The Prediction of Laminarization with a Two-Equation Model of Turbulence," *Int. J. Heat and Mass Transfer*, vol. 15, pp. 301–304, 1972.

[35] M. Gnedin and D. Knight, "A Reynolds Stress Equation Turbulence Model for Compressible Flows. Part I: Flat Plate Boundary Layers." AIAA Paper 95-0860, 1995.

[36] M. Gnedin and D. Knight, "Compressible Turbulence Wall Layer Reynolds Stress Equation Model Version No. 4." Internal Report No. 17, Dept. of Mechanical and Aerospace Engineering, Rutgers University, 1993.

[37] D. C. Wilcox, *Turbulence Modelling for CFD.* DCW Industries, 1993.

[38] W. Jones and B. Launder, "The Prediction of Laminarization with a Two-Equation Model of Turbulence," *Int. Journal of Heat and Mass Transfer*, vol. 15, pp. 301–304, 1972.

[39] S. Dash, D. Wolf, and J. Seiner, "Analysis of Turbulent Underexpanded Jets, Part I: Parabolized Navier Stokes Model SCIPVS," *AIAA Journal*, vol. 23, pp. 505–514, April 1985.

[40] D. Knight, T. Garrison, G. Settles, A. Zheltovodov, A. Maksimov, A. Shevchenko, and A. Vorontsov, "Asymmetric Crossing Shock Wave - Turbulent Boundary Layer Interaction." AIAA Paper 95-0231, January 1995.

[41] D. Knight, D. Badekas, C. Horstman, and G. Settles, "Quasi-conical Flowfield Structure of the Three-Dimensional Single Fin Interaction," *AIAA Journal*, vol. 30, pp. 2809–2816, December 1992.

[42] L. Rosenhead, ed., *Laminar Boundary Layers*, pp. 46–113. New York: Oxford, 1963.

[43] N. Narayanswami, C. C. Horstman, and D. Knight, "Numerical Simulation of Crossing Shock / Turbulent Boundary Layer Interaction at Mach 8.3 - Comparison of Zero- and Two- Equation Turbulence Models." AIAA Paper 93-0779, 1993.

[44] N. Narayanswami, C. C. Horstman, and D. Knight, "Computation of Crossing Shock Turbulent Boundary Layer Interaction at Mach 8.3," *AIAA Journal*, vol. 31, pp. 1369–1376, August 1993.

[45] G.-C. Zha, D. Smith, M. Schwabacher, A. Gelsey, and D. Knight, "High performance supersonic missile inlet design using automated optimization," in *AIAA Symposium on Multidisciplinary Design*, 1996. Submitted, under review.

[46] M. Gnedin, *Numerical Simulation of 3-D Shock Wave Turbulent Boundary Layer Interaction Using a Two Equation Model of Turbulence.* PhD thesis, Rutgers University, May 1996.